

# Adaptation of a solid self-piercing rivet made of aluminum using numerical simulation to extend the application limits

Maximilian Schlicht<sup>1</sup>, Dr.-Ing. Thomas Nehls<sup>1</sup>, Pascal Froitzheim<sup>1</sup>, Prof. Dr.-Ing. Wilko Flügge<sup>1</sup>

<sup>1</sup>Fraunhofer Institute for Large Structures in Production Engineering IGP, Rostock, Germany

## 1 Introduction

Increasing resource efficiency, for example through the consistent application and further development of lightweight construction concepts, plays an important role in the development of the mobility sector. This requires a steadily increasing use of high-strength aluminum alloys in primary vehicle structures. A suitable and efficient process for joining high-strength aluminum alloys is solid self-piercing riveting (SSPR). A major advantage of this process is the elimination of time-consuming preparatory work such as pre-drilling, deburring and positioning of the components to be joined, as the rivet punches through these during the installation process. Due to the high stresses on the rivet during the installation process and the lack of knowledge on the use of ultra-high-strength aluminum alloys as the rivet material, solid self-piercing rivets (SSP-rivets) made of steel are generally used. However, against the background of recyclability, thermal expansion and corrosion protection, the use of aluminum SSP-rivets would be desirable.

To meet the challenges of the joining task, the SSPR can be adapted in terms of material and geometry. In this case, the tool of simulation is very well suited for testing a large number of possible combinations during geometry adaptation and for choosing preferred variants. When mapping the experimental tests and the joining process in the finite element software LS-DYNA®, it is of great importance to characterize the material behavior and failure in appropriate accuracy, in order to be able to physically correctly map the partial aspect of punching in particular.

## 2 Solid self-piercing riveting

Solid self-piercing riveting is a mechanical joining process to join two or more sheets of metal, composite material etc. together by means of a solid rivet. Figure 1 displays the process sequence and the phases of the process curve (Force-Displacement-Curve).

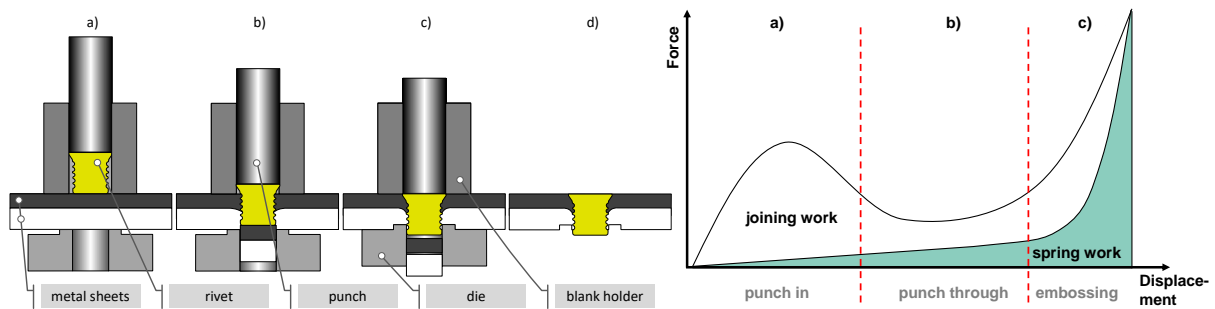


Fig. 1: Steps of the SSPR process (left) and a typical process curve (right)

In the first step (a) the metal sheets are fixed between the blank holder and the die, so that slipping during the joining operation is prevented. The applied preload force depends on the spring used in the tooling. Subsequently (b) the punch presses the solid rivet, which also serves as the cutting punch, through the sheet material. Resulting from the pierced punch sided and die sided material, the slug is discharged through a hole in the die. The punch moves on and presses the countersunk head of the rivet into the punch sided material whereas a flat head is pressed onto the punch sided material (b to c). When the rivet head is flush with the punch sided material, the whole setting unit moves down and with the help of the embossing ring, the die sided material is pressed into the circumferential grooves of the rivet (c). Finally, the punch and the blank holder move up to finish the SSPR process (d). The resulting joint is a form-fit and force-fit connection.

### 3 Geometrical adaptation of the solid self-piercing rivet

Starting point of the investigations was a multigrip rivet from Kerb-Konus-Vertriebs-GmbH with a countersunk head, which is made of the aluminum alloy EN AW-7075 T73. In the following explanations, this rivet is referred to as the “reference” rivet. With this rivet, it is possible to join two sheets of EN AW-6111 PX with a thickness of 1.1 mm each. With a die sided aluminum sheet thickness of 2.0 mm, the grooves are heavily deformed in the joining process, resulting in a “not ok” connection. (c.f. Fig.2)

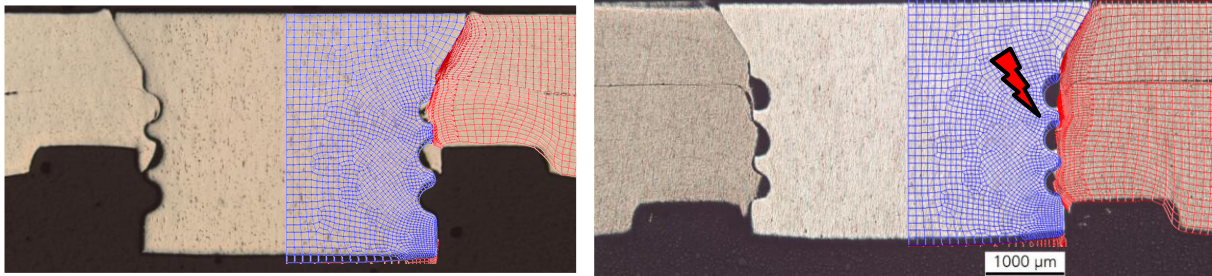


Fig.2: Cross sections of the “reference” rivet with EN AW-6111 PX aluminum sheets; 2 x 1.1 mm (left) and 1.1 mm + 2.0 mm (right)

To overcome the limitations of the reference rivet there are two different approaches: adaptation of the material properties and/or adaptation of the geometric properties. The aluminum alloy AA 7068 in the heat treatment condition T651 was chosen as the new rivet material, as it is one of the highest strength aluminum alloys currently available [1]. The geometric adaptations focus on the geometry of the rivet foot and the geometry of the grooves (c.f. Fig.3). The rivet foot is subjected to high stress, especially in the beginning of the punching process, while the grooves have to withstand high compressive stresses during punching and embossing. The goal is to adapt the geometry of the rivet foot, so that the required force during punching can be reduced and to shape the grooves so that they are not or only slightly deformed during the joining process.

During the project, an attempt was made to improve the rivet foot geometry with the aid of a circumferential chamfer. However, the final project evaluation revealed problems with this rivet foot, so this shape will not be pursued further after the research project, but is seen in all the figures. The procedure for adapting the geometry is to be shown using the groove as an example.

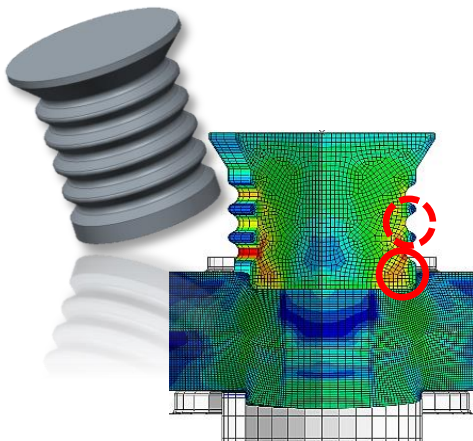


Fig.3: SSP-rivet with marking of the focused areas rivet foot and rivet groove

#### 3.1 Material characterization

To reduce the experimental effort to investigate possible improved geometries of the rivet grooves (e.g. production of the different rivets, extensive sampling) significantly, it is inevitable to use the finite element simulation. In this study, the finite element software LS-DYNA is used for all the numerical investigations. The first step is to determine the fundamental material properties of the aluminum alloys used. For this purpose, tensile tests were carried out. Flat tensile specimens were used for the aluminum sheets and round tensile specimens for the aluminum material of the solid rivets, both according to DIN 50125 [2]. Some parameters, like the e-module and the yield stress, can be directly transferred into the used material model \*024-PIECEWISE\_LINEAR\_PLASTICITY (“\*MAT\_024”), which is commonly used in

LS-DYNA to map the elastic-plastic behavior of metals in a simplified way [3]. The simplicity allows a stable and low computational calculation with good accuracy. In order to be able to map the high degrees of deformation that occur during the SSPR process in the simulation, it is necessary to define a flow curve, in which the flow behavior beyond the yield point at high degrees of deformation is characterized. Therefor the received results from the tensile tests were extrapolated with an appropriate mathematical approach for each of the materials, where in the case of EN AW-6111 PX a softening following [4] is taken into account (c.f. Fig.4). The curves were then deposited in the corresponding material card.

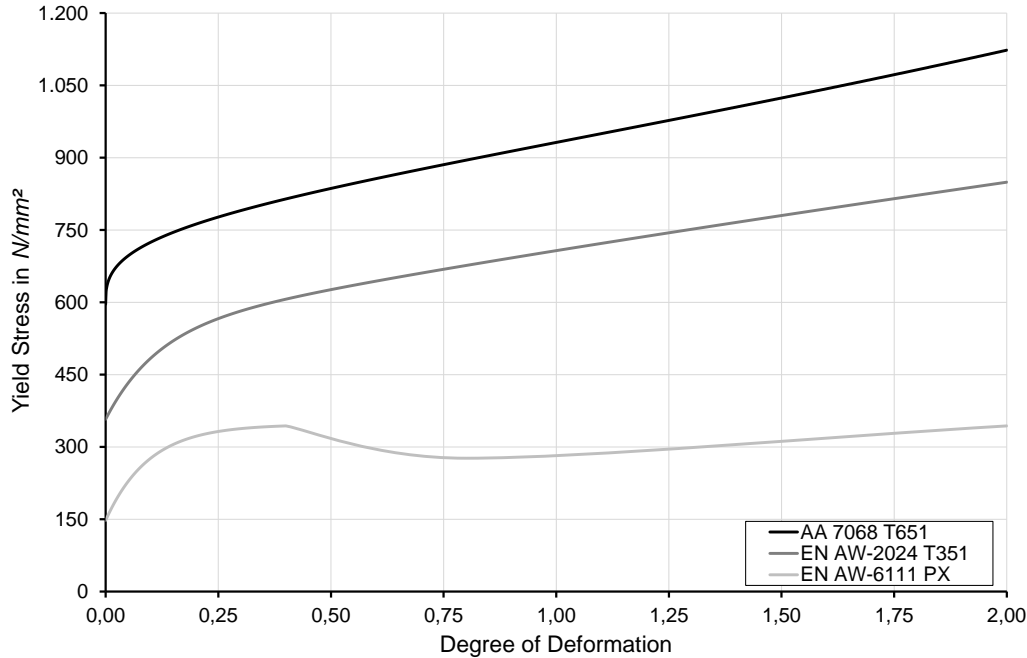


Fig.4: Extrapolated flow curves for the aluminum alloys

Since material separation is an important element in the SSPR process, a damage model is required that can represent the physical phenomena in the process with sufficient accuracy within the simulation. The model used in this research is GISSMO (“generalized incremental stress state dependent model”) [5]. In this model, the damage increases incrementally depending on the stress state of the respective element:

$$\Delta D = \frac{DMGEXP * D^{(1-\frac{1}{DMGEXP})}}{\varepsilon_f(\eta)} \Delta \varepsilon_p \quad (1)$$

$D$	<i>damage variable</i>	$DMGEXP$	<i>damage parameter</i>
$\varepsilon_f$	<i>(equivalent) failure strain</i>	$\Delta \varepsilon_p$	<i>increment plastic strain</i>

The stress state is characterized by

$$\eta = \frac{\sigma_H}{\sigma_{vM}} \quad (2)$$

$\sigma_H$	<i>hydrostatic pressure</i>	$\sigma_{vM}$	<i>equivalent stress according to v. Mises</i>
------------	-----------------------------	---------------	--

Advantages of this damage model are the consideration of effects of instability and a possible implementation of a mesh dependence. To benefit from these advantages and map the material behavior of the aluminum appropriately, the parameters of GISSMO, especially the FADEXP and the failure strain, should be iteratively adapted to a wide selection of basic material tests (layer crush test, shear tests, tensile tests). In the research project, such a large test scope for adapting the material failure behavior was not planned, so that, in a first try, GISSMO was adapted only based on tensile test data. This was to find out, whether sufficient accuracy could be achieved in the simulation and whether it is suitable as a tool for mapping trends.

Based on the experimental investigations, tensile test with a flat tensile specimen for the aluminum sheets were modeled in LS-DYNA (c.f. Fig.5). In this case, a quarter model is sufficient due to the existing symmetries. 3D fully integrated shell elements (**ELFORM 16**) were used to describe the specimen geometry. The element edge length was defined as 1.0 mm, 0.5 mm and 0.1 mm respectively.

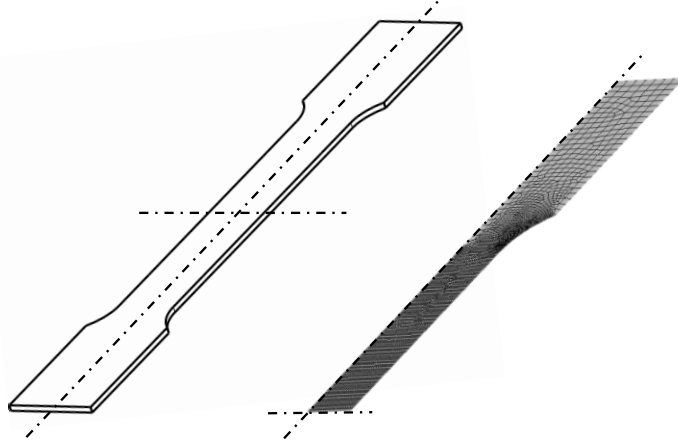


Fig.5: Geometry of the tensile specimen (left) and simulation model of the tensile specimen (right)

The simulation was calculated with the version **mpp\_s\_R10.0.0** of the LS-DYNA solver in an explicit procedure. The results of the simulation were iteratively adapted to the Force-Displacement-Curves of the experimental results for each element edge length. Figure 6 shows the obtained curves and fracture patterns of the simulations and the experiments using the aluminum EN AW-6111 PX with a thickness of 2.0 mm as an example.

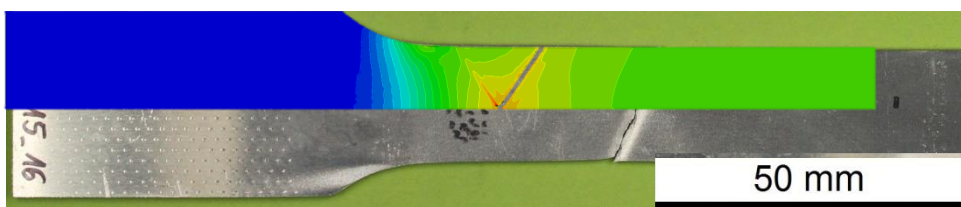
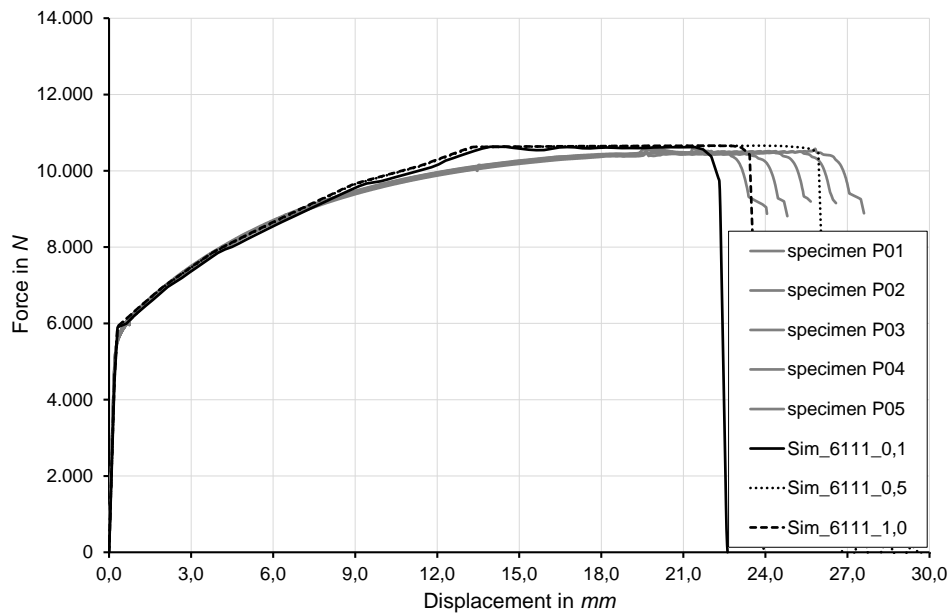


Fig.6: Experimental and numerical results of the tensile tests with EN AW-6111 PX  $t = 2.0$  mm; Force-Displacement-Curves (top) and fracture pattern (bottom)

The comparison of the results proves a good agreement between the simulations with the iteratively adapted GISSMO damage model and the tensile tests. The force-displacement curves of the simulations reproduce the course of the experimental curves well and lie within the experimental scatter range at

the point of specimen failure. With the help of the GISSMO damage model it is possible to recreate a certain localization of the damage but the precise place of failure can't be predicted. However, the course of the failure for the aluminum alloys can be predicted with high accuracy.

The same investigations were carried out for the other aluminum sheet material EN AW-2024 T351 and for the rivet aluminum AA 7068 T651. The results also showed good agreements between experiment and simulation. With the help of the determined parameters and the flow curves, it is now possible to perform further investigations using the adjusted GISSMO damage models.

### 3.2 Groove stripping tests

The goal of the geometrical improvement of the rivet groove is to increase its shear strength. When punching through the sheets, minor deformations of the groove are permissible to the extent that they can continue to fulfill their function. However, deformation is not permissible during embossing. To adapt the groove geometry for these requirements three different groove geometries were chosen and modeled, as seen in Figure 7. The small area of the groove is of special interest, so very small elements of 0.03 mm to 0.09 mm were used to describe the geometry of the groove accurately.

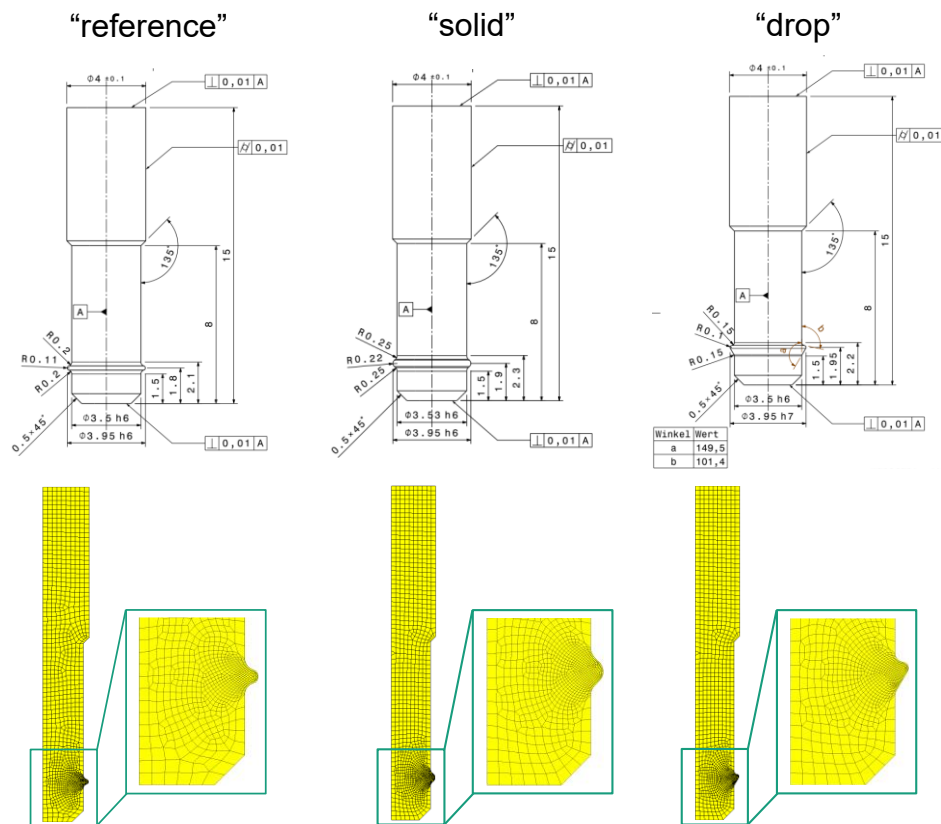


Fig.7: Chosen groove geometries for the groove stripping tests

In order to get a deeper knowledge on how the rivet groove is loaded in the crucial phase of the joining process and to exclude influences e.g. from the rivet foot, simplified groove stripping test were carried out, where the rivet was replaced with an aluminum punch (c.f. Fig.7).

For the numerical investigations, a 2D rotationally symmetric model was set up (c.f. Fig.8). At the same time, experiments were performed to verify and control the determined parameters of the GISSMO damage model. The simulation is built with rotationally symmetric shell elements (**ELFORM 15**). Tools (punch, blank holder, die) are defined as rigid while the aluminum punch and sheet ( $t = 2.5$  mm) are defined with an elastic-plastic material behavior (**\*MAT\_024**). The chosen contact is a penetration based 2D surface-to-surface contact (**\*CONTACT\_2D\_AUTOMATIC\_SURFACE\_TO\_SURFACE**) with a Coulomb friction model (**FS = 0.10**). The movement of the punch is defined with a Displacement-Time-Curve (**\*BOUNDARY\_PRESCRIBED\_MOTION\_RIGID**) which represents the specified punch speed set on the testing machine.

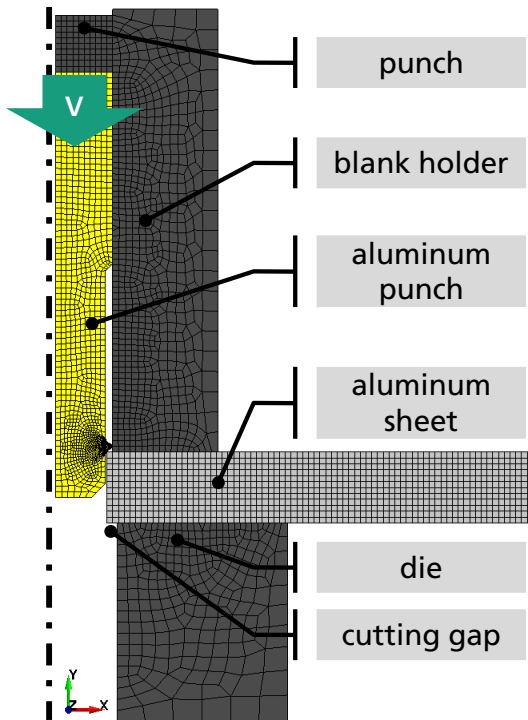


Fig.8: 2D rotationally symmetric simulation model of the groove stripping tests

The following Figures 9, 10 and 11 show the experimental and numerical results of the groove stripping tests:

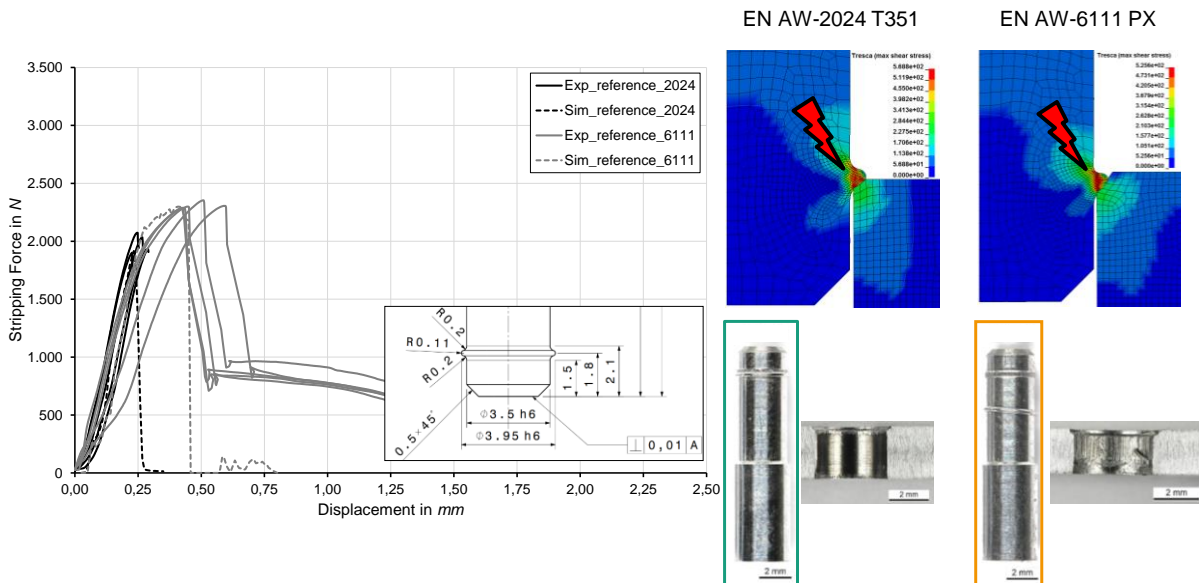


Fig.9: Experimental and numerical results of the groove stripping test with the groove geometry “reference”; Force-Displacement-Curves (left) and failure pattern (right)

The Stripping Force-Displacement-Diagram (c.f. Fig.9) of the “reference” groove geometry shows a very good agreement between experiments and simulation in terms of maximum stripping force, time and characteristics of groove failure. The simulation is therefore able to describe the shearing of the groove as well as the earlier failure with the aluminum sheet EN AW-2024 T351 due to its higher strength and higher resistance against the aluminum punch with the groove moving downward.

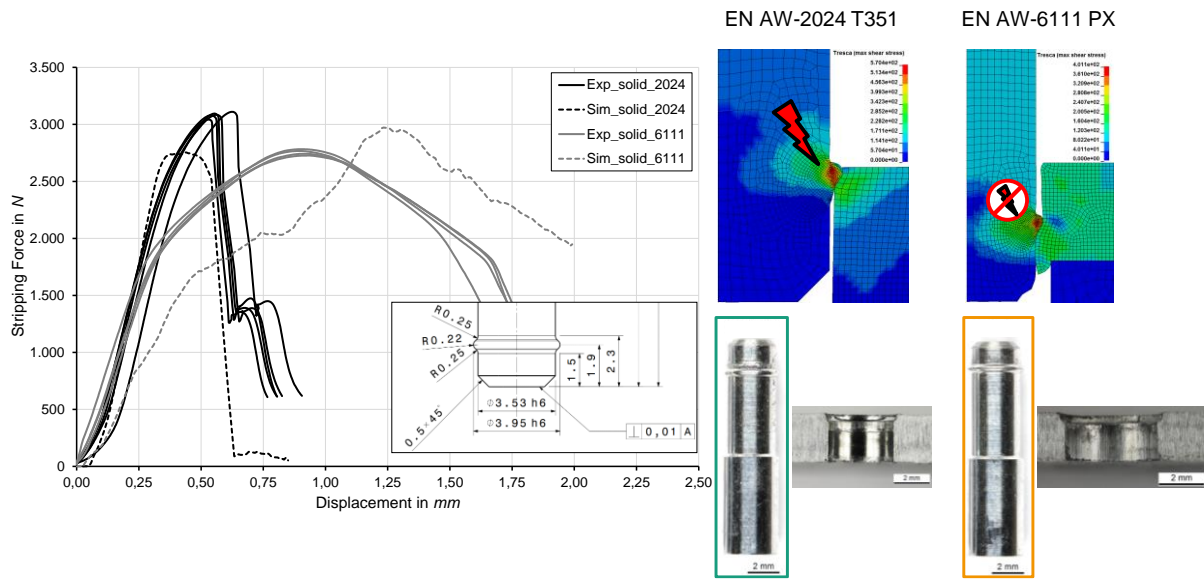


Fig. 10: Experimental and numerical results of the groove stripping test with the groove geometry “solid”; Force-Displacement-Curves (left) and failure pattern (right)

With the “solid” groove geometry, the simulation cannot exactly reproduce the experimental findings (c.f. Fig.10). With the EN AW-2024 T351 sheets, the simulation underestimates the maximum stripping force. The adjusted GISSMO isn’t quite able to predict the failure behavior under the prevailing loads. On the other hand, the time of the drop of the force due to the tear-off of the groove is covered well. With the EN AW-6111 PX sheets, the groove doesn’t fail during the test, therefore resulting in a different curve, especially after the maximum stripping force is reached. The offset of the process curves shows that the material behavior, under this kind of load without groove failure, is only approximately described but depicts the experiments sufficiently accurately.

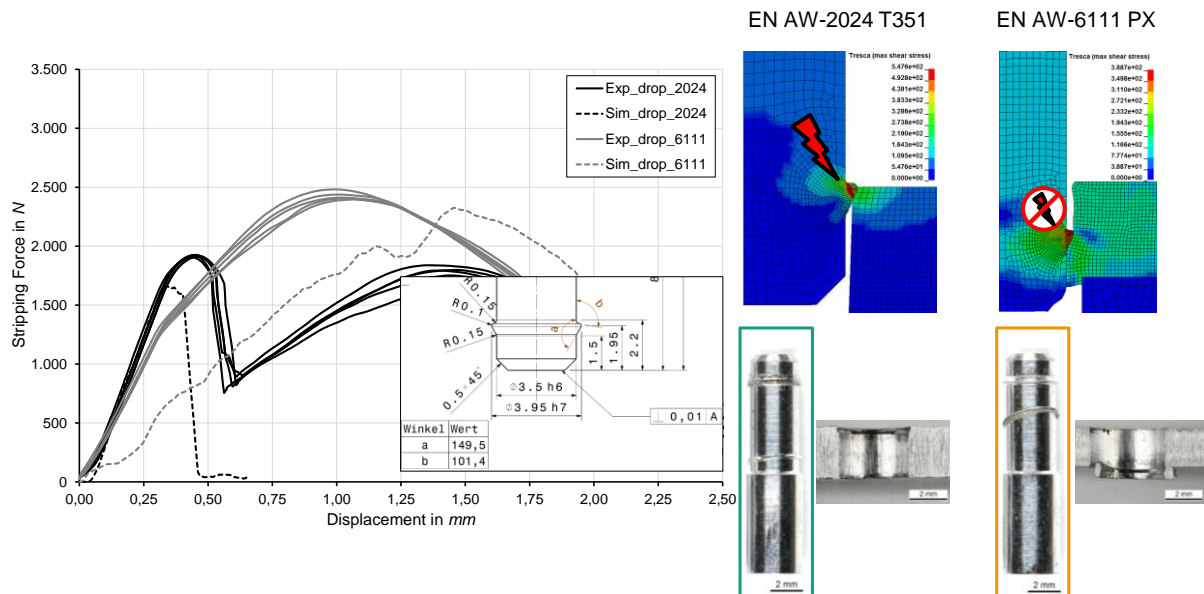


Fig. 11: Experimental and numerical results of the groove stripping test with the groove geometry “drop”; Force-Displacement-Curves (left) and failure pattern (right)

The comparison of the experiments and the simulations with the “drop” rivet groove geometry shows a similar deviation of the numerical results as with the “solid” geometry (c.f. Fig.11). With the EN AW-2024 T351 sheets, the simulation underestimates the maximum stripping force but can describe the failure characteristics in good agreement. This rivet groove geometry also does not fail in combination with sheets made of EN AW-6111 PX. The numerical obtained curve shows an offset to the experimental curves due to the above-mentioned reasons.

From the results of the investigations, it is evident that the “stable” rivet groove geometry can withstand the highest stripping forces. Therefore, it was selected as the preferred variant.

In conclusion, the simulation slightly underestimates the maximum stripping forces reached during the groove stripping tests. The parameters of the material model were verified even not all effects and curves could be exactly depicted. Deviations result mainly from the element formulation, the element deletion used for material separation and the only approximately depicted material behavior. Overall it was shown, that the simulation is suited enough for this and following investigations.

#### 4 Validation of the adaptation

The results of the previous investigations regarding the rivet groove geometry and rivet foot geometry were combined into two new rivet geometries: a countersunk head rivet and a flat head rivet (c.f. Fig.12). The former is intended for use in the automobile industry while the latter is intended for use in aircraft construction. Both are made of the chosen aluminum alloy AA 7068 T651.

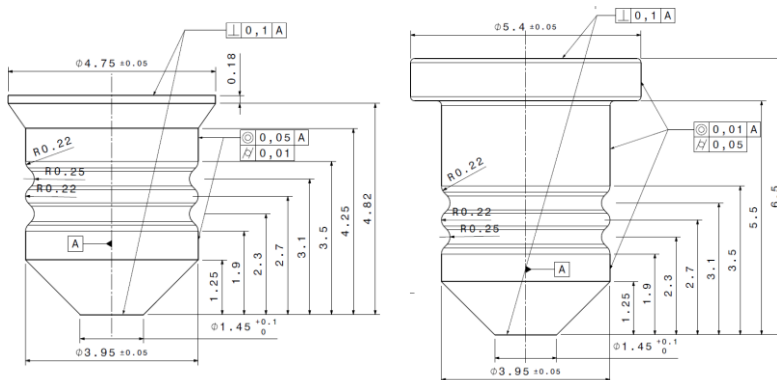


Fig.12: Drawings of the countersunk head rivet (left) and the flat head rivet (right)

The used simulation model is shown in Figure 13 with the countersunk head rivet as an example. Following the preliminary investigations, the simulation model is set up 2D rotationally symmetrical with shell elements (**ELFORM 15**). Tools are modelled as rigid. Aluminum sheets and the rivet are defined with an elastic-plastic (**\*MAT\_024**) with the GISSMO damage model activated for the sheets. The contact definition is a 2D-surface-to-surface contact. The friction parameter is slightly adjusted to  $\mu_s = 0.21$ . The punch velocity is set to 1.685 mm/s with regard to the experiments.

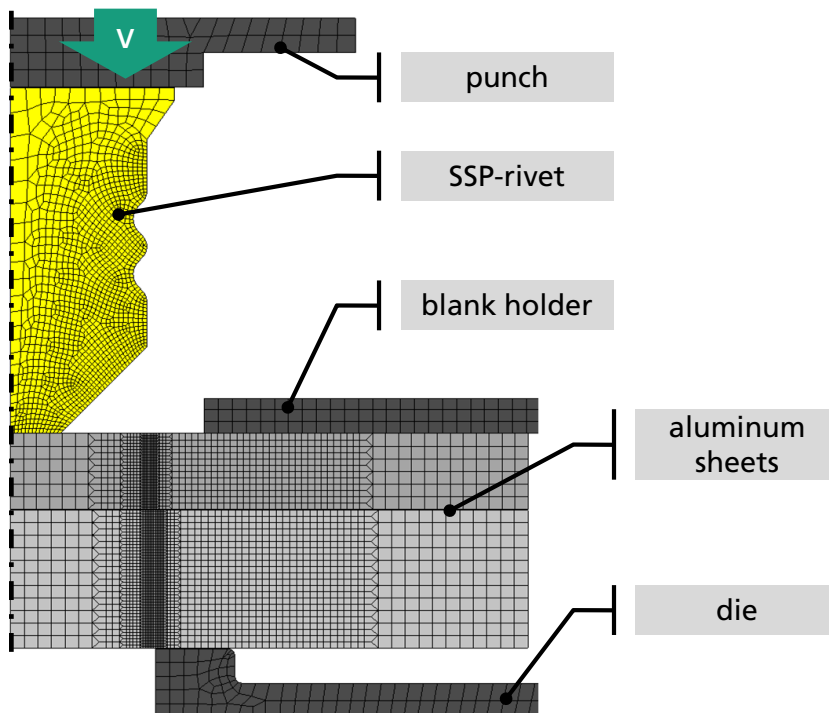


Fig.13: 2D rotationally symmetric simulation model of the SSPR process with the countersunk head rivet

In a first iteration, this model was used to identify a die geometry and to get the best joining result for the two rivets without having to conduct extensive, time-consuming experiments. The inner diameters of the die were varied from 4.2 mm to 4.5 mm, each die having an adapted embossing ring geometry. Aluminum sheets EN AW-6111 PX in the combination 1.1 mm + 2.0 mm and 2 x 2.0 mm were used.

The examinations with the countersunk head rivet (c.f. Fig.14 left) show, that with a larger die inner diameter the groove filling level is significantly lower and the punch sided sheet is not sufficiently pressed against the rivet shaft. This weakens the form-fit of the connection. With a reduced die inner diameter, the rivet grooves are subjected to higher stresses, but only in the elastic range. A die inner diameter of 4.2 mm was chosen as the best variant.

The investigations with the flat head rivet (c.f. Fig.14 right) indicate, that with a larger die inner diameter the stress on the rivet grooves and the groove filling level decrease. This rivet variant tends to be compressed in the joining process and thus to bulge. This phenomenon increases with decreasing die inner diameter. Due to these opposing effects, it was not clearly possible to select a preferred variant. Due to the element deletion to represent the material failure in the simulation, the variant with the 4.5 mm die inner diameter seemed to be the most promising.

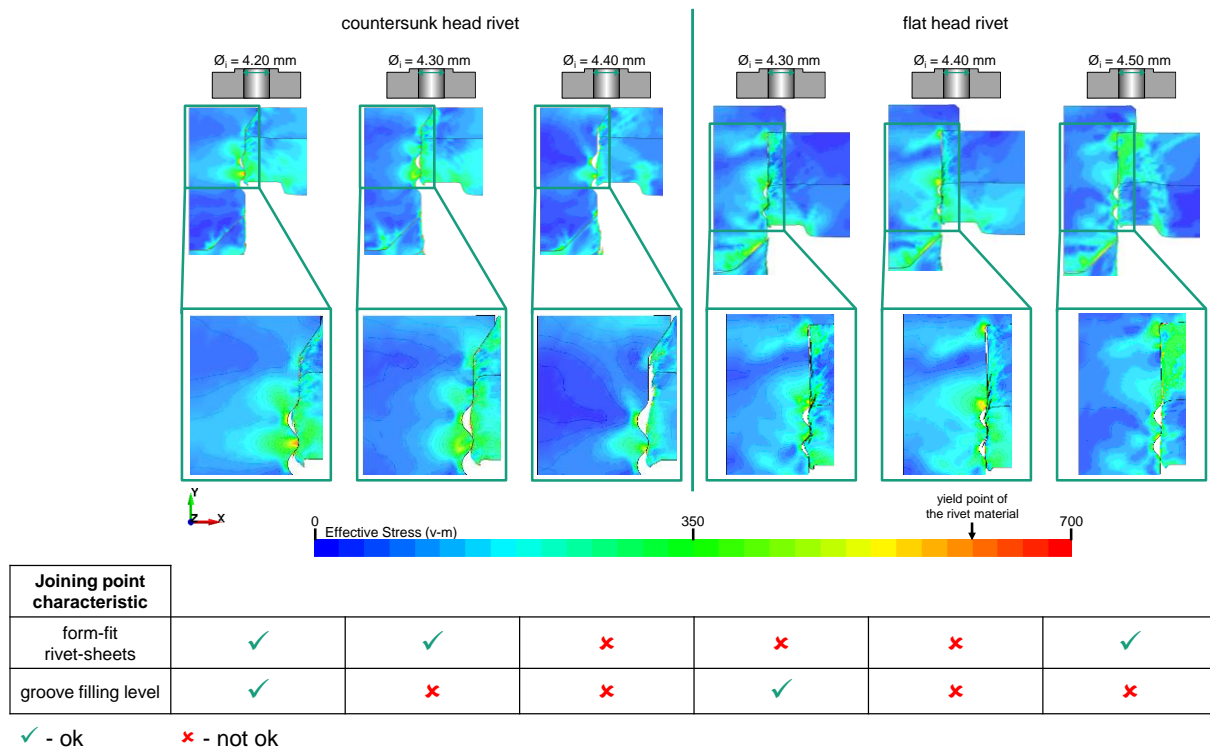


Fig.14: Joining point characteristics and rivet groove stress with different die geometries; countersunk head rivet (left) and flat head rivet (right)

The selected die variant for each rivet was used in further experimental investigations. The material combination 1.1 mm + 2.0 mm EN AW-6111 PX was used together with the countersunk head rivet, while the flat head rivet was used to join 2 x 2.0 mm EN AW-6111 PX. The curves from the joining process were recorded to compare them to the curves from the simulation (c.f. Fig.15 right). To compare the joint characteristics, joining point samples were prepared and the geometry of the joints from the simulation were superimposed on the cross sections of the experimental joints (c.f. Fig.15 left).

The simulation with the countersunk head rivet and the flat head rivet basically show a good approximation of the joining point characteristics. Both simulations show an underestimation of the compression of the rivet. Reasons for this could be, that the flow curves of the materials are derived only from tensile test data and that the GISSMO failure strain curve for the aluminum sheets has not been sufficiently adapted to test data under other types of loads. Therefore, the material behavior and failure are only approximately depicted in the simulation. In contrast to the experiments, the simulation isn't quite able to depict the groove filling level accurately due to the element deletion that is used to consider the material failure in the simulation. Despite this, the simulation can show a tendency of the characteristics of the joining points.

Regarding the process curves, the simulation is able to show the characteristics of the joining process. Due to a lack of an implementation of the machine stiffness by installing springs in the simulation model, the force gradient of the numerical plotted curves is significantly higher resulting in a small deviation between the experimentally and numerically achieved displacement. The earlier mentioned element deletion leads to an underestimation of the stress in the phase of punching through, since the frictional stress between the rivet groove and the aluminum sheets cannot be represented in this phase. The use of an element edge separation could lead to an improvement in the simulation but was not applicable in connection with the GISSMO failure model at the time of the investigations. In contrast, important parameters like the maximum punching force and the embossing force are mapped in good approximation.

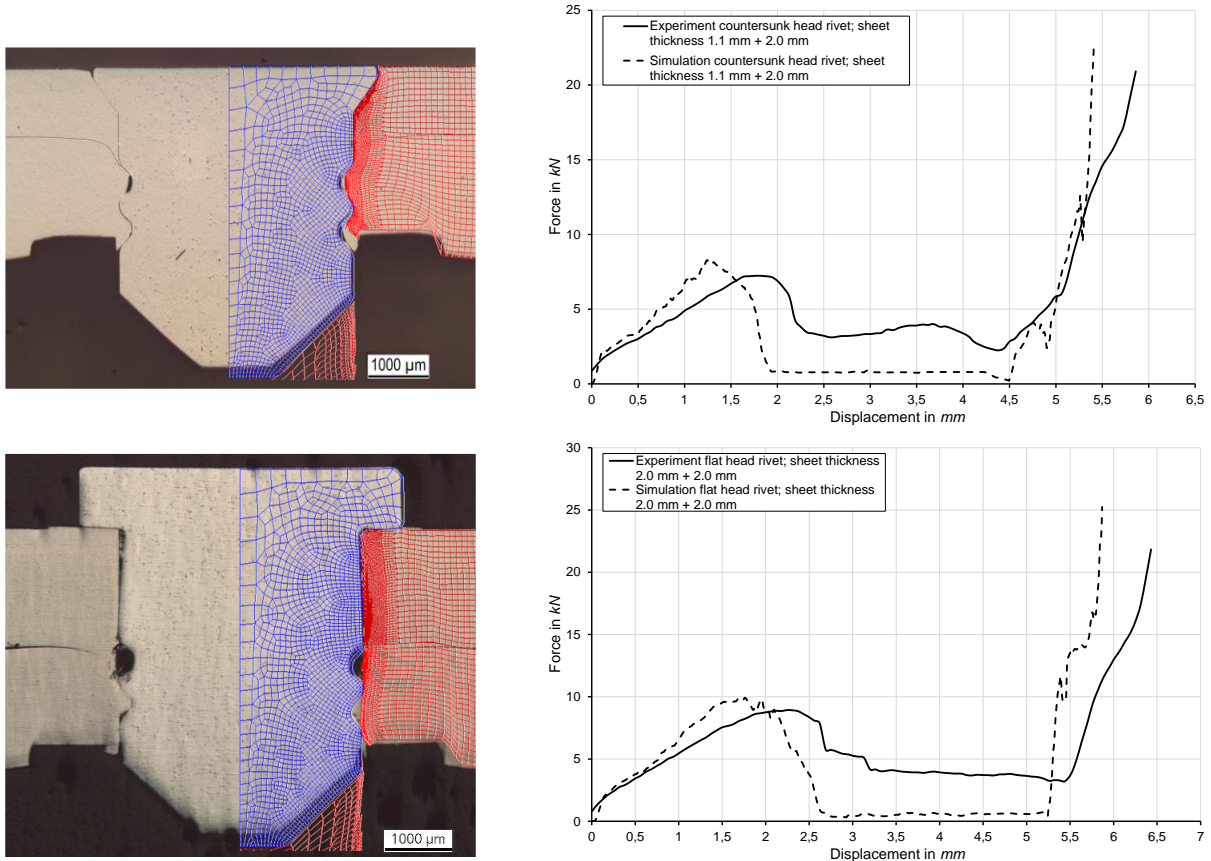


Fig. 15: Superimposition of the cross sections of the set joining points with the mesh from the simulations and comparison of the Force-Displacement-Curves of the experiments and the simulations; countersunk head rivet (top) and flat head rivet (bottom)

## 5 Summary

The aim of these investigations was to geometrical adapt a “reference” SSP- rivet made of aluminum to extend the application limits for joining aluminum sheets. In order to keep the experimental effort significantly within limits, numerical simulation with the finite element program LS-DYNA was used. To map the material behavior of the materials, experimental data from tensile tests were extrapolated into flow curves. Since the SSPR process involves material separation during punching through, a damage model was needed, that can depict this process in the simulation. Therefore, the GISSMO damage model was used and calibrated on the tensile test data in a first simulation run. The simulations of the tensile tests were in good agreement with the experiments. To adapt the rivet groove geometry, simplified groove stripping tests were carried out. A 2D rotationally symmetric model was built in LS-DYNA. The numerical results were in acceptable agreement with the experimental results. Important effects and trends between the different variants could be seen in the simulation. The most suitable rivet groove variant was chosen and transferred to a countersunk head rivet and a flat head rivet, each for different use cases. With the help of a 2D rotationally symmetric simulation model of the joining process, the most suitable die geometry was identified without great experimental effort. A comparison between the experimental and numerical results of the final variants of joining processes with the countersunk head rivet and the flat head rivet indicated that the simulation is able to depict trends and most of the

core properties of the joining process. Deviations occurred from the used element deletion to show material failure and the adjustment of the material behavior only to data from tensile tests. With the help of the described procedure it was possible to extend the application limit for joining aluminum sheets from 2 x 1.1 mm EN AW-6111 PX to 1.1 mm + 2.0 mm and 2 x 2.0 mm EN AW-6111 PX respectively. In conclusion, the built simulation models map the experimental results in a satisfactory accuracy, so that the application limits of an aluminum rivet could be extended significantly. Potential for improvements lies in the mapping of the machine stiffness within the simulation, the use of an element edge separation instead of an element deletion and a more comprehensive material characterization to increase the accuracy of the adaptation of the GISSMO damage model. These improvements should lead to a higher mapping accuracy, which would again significantly expand the applicability of the aluminum rivet.

## 6 Literature

- [1] Nowak, K., Osten, J., Nehls, T., Schlicht, M., Fuchs, N., Reich, M.: "Fügen von Strukturbauteilen aus hochfesten Aluminiumknetlegierungen durch Vollstanznieten aus höchstfesten Aluminiumlegierungen (Aluminium Vollstanznieten)", IGF-Schlussbericht, 2019
- [2] DIN 50125:2016-12: "Prüfung metallischer Werkstoffe – Zugproben", 2016
- [3] LSTC: "Keyword User's Manual – Volume II: Material Models", R12, 2020
- [4] Doege, E., Meyer-Nolkemper, H., Saeed, I.: "Fließkurvenatlas metallischer Werkstoffe – Mit Fließkurven für 73 Werkstoffe und einer grundlegenden Einführung", 1986
- [5] Neukamm, F., Feucht, M., Haufe, A.: "Considering damage history in crashworthiness simulations", 7<sup>th</sup> European LS-DYNA Conference, 2009